Spectroscopic investigation and crystal field modelling of Dy^{3+} and Er^{3+} energy levels in yttrium aluminium borate (YAB) single crystals

2005 J. Phys.: Condens. Matter 17 6245

(http://iopscience.iop.org/0953-8984/17/39/010)

INSTITUTE OF PHYSICS PUBLISHING JOURNAL OF PHYSICS: CONDENSED MATTER

J. Phys.: Condens. Matter **17** (2005) 6245–6255 doi:10.1088/0953-8984/17/39/010

Spectroscopic investigation and crystal field modelling of Dy^{3+} and Er^{3+} energy levels in yttrium aluminium borate (YAB) single crystals

A Baraldi[1], R Capelletti[1], N Magnani[1], M Mazzera[1], E Beregi[2] and I Földvári[2]

[1] Department of Physics, University of Parma and Consorzio Nazionale Interuniversitario di Scienze Fisiche della Materia (CNISM), Parco Area delle Scienze 7A, 43100 Parma, Italy
[2] Research Institute for Solid State Physics and Optics, HAS, Konkoly-Thege u. 29-33, 1121 Budapest, Hungary

Received 24 June 2005, in final form 30 August 2005
Published 16 September 2005
Online at stacks.iop.org/JPhysCM/17/6245

Abstract

High resolution (0.04 cm^{-1}) absorption spectra of Dy^{3+}-doped $YAl_3(BO_3)_4$ (YAB) single crystals were measured by Fourier transform spectroscopy in the spectral (2000–23 000 cm^{-1}) and temperature (9–300 K) ranges. Samples with nominal 1 and 4% Dy/Y molar ratios were studied. Dy^{3+} transitions from the $^6H_{15/2}$ ground state to the $^6H_{13/2}$, $^6H_{11/2}$, $^6H_{9/2}$ + $^6F_{11/2}$, $^6H_{7/2}$ + $^6F_{9/2}$, $^6H_{5/2}$, $^6F_{7/2}$, $^6F_{5/2}$, $^6F_{3/2}$, and $^4F_{9/2}$ excited states were analysed. A small (∼3.3 cm^{-1}) splitting between the first two sublevels of the $^6H_{15/2}$ ground manifold was detected. The experimentally determined energy levels were fitted with a single-ion Hamiltonian and the crystal-field parameters were obtained. The same procedure was applied to analyse the previously published high resolution spectra of YAB:Er^{3+}, leading to a reliable unified picture for the two dopants.

1. Introduction

$YAl_3(BO_3)_4$ (YAB) is an interesting representative of the self-frequency doubling laser hosts. Favourable physical parameters, such as broad transparency range (down to 200 nm), good incorporation of rare earth ions, large nonlinear optical coefficients, and proper refractive index dispersion for phase matching, have encouraged its investigation in view of relevant applications [1]. Several rare-earth-doped YAB crystals were successfully grown and studied [2, 3]. In Nd-doped YAB (NYAB) laser action has already been demonstrated [4] and self-frequency doubling has been reported [5]. The spectroscopic analysis of Dy^{3+} in YAB crystals was performed by means of absorption and luminescence measurements [6, 7]: unusually large differences were reported between the measured and calculated peak positions. This might be due to the complexity of the Dy^{3+} spectra, to the small difference expected between the first two Stark sublevels of the ground $^6H_{15/2}$ state [7], and to the standard spectral resolution of the employed spectrometers. For the Dy^{3+} energy level calculations based on

the experimental data fitting the root mean square (RMS) deviation of the calculated values from the experimental ones ($\sigma = 14\ \mathrm{cm}^{-1}$) was close to the width of the measured lines [7]. This suggests that the fitting quality might be improved by significantly increasing the spectral resolution. For the YAB:Er^{3+} system the high resolution absorption spectra in the range 6000–23 000 cm^{-1} have already been published [8, 9], while standard resolution spectra have been reported up to 27 500 cm^{-1} [10]. However, the only calculated energy levels for Er^{3+} in YAB available in the literature [11] were obtained by fitting standard resolution spectroscopic data.

The purpose of the present paper is to demonstrate how high resolution spectra are the necessary background to improve crystal field model calculations for rare earth ions in YAB. Therefore high resolution Fourier-transform absorption spectroscopy was applied in the temperature range 9–300 K to investigate the YAB:Dy system. In the case of YAB:Er high resolution experimental data, already published [8, 9], were used to evaluate the crystal field parameters.

2. Experimental techniques and theoretical modelling

YAB single crystals were grown by the top-seeded flux method from $K_2O/MoO_3/B_2O_3$ flux. Detailed experimental conditions can be found in [12]. The Dy dopant was added as Dy_2O_3. The YAB:Dy crystals were of nearly stoichiometric composition. Crystals with nominal 1 and 4% Dy/Y molar ratios were grown for the present investigation. The segregation coefficient of Dy in the YAB crystal/flux system was close to unity and the Dy concentration along the crystal was homogeneous. According to the atomic absorption analysis, the actual Dy concentrations in the crystals were close to the nominal ones [13]. Traces of unwanted impurities, as Cr^{3+}, were detected in the 1% Dy:YAB sample by monitoring the two very weak R1 and R2 lines, originated by the Cr^{3+} $^4A_2 \rightarrow {}^2E$ crystal field transition, at 14 633.6 and 14 689.9 cm^{-1}, respectively, in the 9 K absorption spectrum [14, 15]. Possible traces of flux elements (e.g. Mo) may be present as well [10]. Preliminary optical microscope analysis of the samples between crossed polarizers showed striations which might be interpreted, in agreement also with previous observations [16], as due to twinning and/or to inner strain fields.

For the spectroscopic investigations, the crystals were x-ray oriented, cut and polished. The oriented samples were z- and x-cuts. The sample thickness was about 2 mm. The optical absorption spectra were monitored by a Bomem DA8 Fourier transform spectrometer operating in the spectral range 2000–23 000 cm^{-1} with a resolution as fine as 0.04 cm^{-1}. The sample temperature was varied between 9 and 300 K by assembling the sample in a 21SC Model Cryodine Cryocooler of CTI Cryogenics equipped with KRS5 and quartz windows. Measurements with linearly polarized light were performed by using a gold grid polarizer deposited onto a KRS5 substrate.

The experimentally determined energy levels were fitted with a single-ion Hamiltonian that accounts for free-ion and crystal-field interactions. According to [17], the atomic part is written as

$$H_{\mathrm{FI}} = E_{\mathrm{av}} + \sum_k F^k f_k + \zeta H_{\mathrm{SO}} + \alpha L(L+1) + \beta G(G_2) + \gamma G(R_7) + \sum_i T^i t_i + \sum_j M^j m_j + \sum_k P^k p_k \quad (1)$$

where $k = 2, 4, 6$; $i = 2, 3, 4, 6, 7, 8$; $j = 0, 2, 4$. This model free-ion Hamiltonian accounts for two-body electrostatic repulsion (F^k), two- and three-body configuration interactions (α, β, γ, and T^i, respectively), spin–orbit coupling (ζ), spin–other-orbit interactions (M^j),

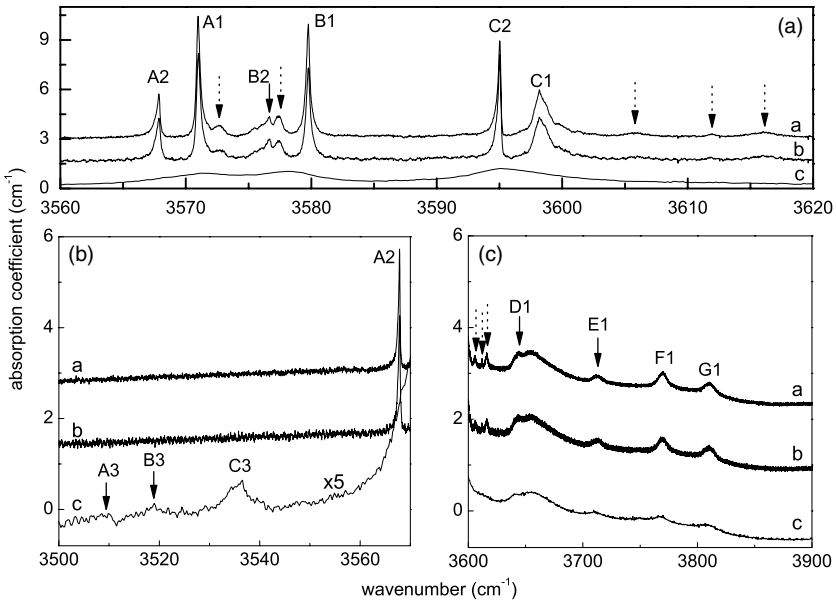

Figure 1. Absorption spectra of 1% Dy:YAB sample (x-cut) in the region of the $^6H_{15/2} \rightarrow {}^6H_{13/2}$ transition (the three panels cover the whole 3500–3900 cm^{-1} range) measured at different temperatures T. Curve a, $T = 9$ K; curve b, $T = 20$ K; curve c, $T = 100$ K. The resolution is 0.04 cm^{-1} for curves a and b, and 0.5 cm^{-1} for curve c. The dotted arrows indicate some additional lines.

and electrostatically correlated spin–orbit interactions (P^k); the spherically symmetric one-electron contribution is represented by a uniform energy shift of the $4f^n$ configuration (E_{av}). More detailed descriptions of the various operators and parameters, which have become quite standard, are available in the literature [18]. The crystal-field Hamiltonian for D_3-symmetry sites is written as

$$H_{CF} = B_2^0 C_0^{(2)} + B_4^0 C_0^{(4)} + B_4^3 (C_{-3}^{(4)} - C_{+3}^{(4)}) + B_6^0 C_0^{(6)} + B_6^3 (C_{-3}^{(6)} - C_{+3}^{(6)}) + B_6^6 (C_{-6}^{(6)} - C_{+6}^{(6)}) \tag{2}$$

in terms of the tensor operators $C_q^{(k)}$ defined in [19] (the B_k^q parameters are expressed according to Wybourne's normalization).

3. Results and discussion

3.1. YAB:Dy

The high resolution absorption spectra of YAB:Dy crystals were measured in the 2000–23 000 cm^{-1} range. An example is portrayed in figure 1. The nine expected transitions from the ground $^6H_{15/2}$ state to the excited $^6H_{13/2}$, $^6H_{11/2}$, $^6H_{9/2} + {}^6F_{11/2}$, $^6H_{7/2} + {}^6F_{9/2}$, $^6H_{5/2}$, $^6F_{7/2}$, $^6F_{5/2}$, $^6F_{3/2}$ and $^4F_{9/2}$ manifolds of Dy^{3+} were detected. The number of sublevels predicted by the Kramers' theorem is $(2J + 1)/2$ for each manifold. By analysing the spectra related to both Dy concentrations (see the previous section), all the transitions from the lowest sublevel of the ground state to the $(2J+1)/2$ sublevels of the excited manifolds were identified, except for a very few lines; see table 1. The lines could be distinguished not only by exploiting the high resolution and the low temperature induced line narrowing, but also by performing

Table 1. Comparison between the theoretical and experimental values of Dy^{3+} energy levels (cm^{-1}) in the 1% Dy:YAB crystal sample (x-cut) for different $^{2S+1}L_J$ manifolds.

$^{2S+1}L_J$	Level	Theoretical[a]	Exp.[a]	Exp.[b]	Exp.[c]
$^6H_{15/2}$	1	2.0	0	0	0
	2	10.9	3.3 ± 0.2	10	—
	3	71.3	62.9 ± 1.9	75	70
	4	219.0	—	228	227
	5	268.5	—	305	—
	6	331.2	—	336	322
	7	418.6	—	425	416
	8	465.6	—	468	458
$^6H_{13/2}$	A	3559.7	3570.98	3571	—
	B	3587.7	3579.76	3598	3580
	C	3588.1	3598.18	3650	3586
	D	3640.3	3644.07	3687	3608
	E	3700.7	3712.48	3716	3658
	F	3757.7	3769.82	3771	3725
	G	3802.5	3810.41	3810	3778
$^6H_{11/2}$	A	5842.2	5846.18	5844, 5847	5860
	B	5945.3	5946.72	5948	—
	C	5985.3	5990.2	5962	5961
	D	6040.6	6038.77	5989, 5993	6006
	E	6047.2	6046.73	6037	—
	F	6048.8	6047.96	6049	6064
$^6H_{9/2} + {}^6F_{11/2}$	A	7680.8	7692.21	7695	—
	B	7717.8	7713.90	7713, 7717	7714
	C	7734.2	7736.10	7738	7731
	D	7767.8	7756.92	7754, 7758	7756
	E	7813.4	7810.72	7791	7777
	F	7830.3	7819.00	7813	7836
	G	7835.9	7844.44	7820, 7826	—
	H	7886.5	7875.53	7877	—
	L	7968.2	7963.87	7897	7991
	M	8000.2	7984.06	7966	—
	N	8036.7	8023.50	7986	8045
$^6H_{7/2} + {}^6F_{9/2}$	A	9045.9	9047.14	9047	9041
	B	9065.2	9069.86	9071	9058
	C	9108.3	9111.41	9113	9099
	D	9189.7	9189.50	—	9182
	E	9193.8	9192.75	9191	—
	F	9250.0	9244.78	9246	9242
	G	9321.4	9320.71	9323	9328
	H	9346.7	9335.47	9338	9337
	L	9358.8	9348.93	9351	9389
$^6H_{5/2}$	A	10 217.1	10 208.6	—	—
	B	10 276.6	10 282.5	10 285	10 288
	C	10 429.0	10 423.1	10 426	10 373
$^6F_{7/2}$	A	11 055.9	11 042.9	11 043	11 047
	B	11 086.1	11 093.3	11 095	—
	C	11 087.2	11 094.5	11 143	11 101
	D	11 131.9	11 143.7	11 146	11 150

Table 1. (Continued.)

$^{2S+1}L_J$	Level	Theoretical[a]	Exp.[a]	Exp.[b]	Exp.[c]
$^6F_{5/2}$	A	12 432.9	12 425.3	12 428	12 434
	B	12 472.9	12 484.6	12 489	12 493
	C	12 515.1	12 525.2	12 529	12 534
$^6F_{3/2}$	A	13 264.3	13 268.6	13 269, 13 273	13 276
	B	13 276.3	13 281.5	13 285	13 290
$^6F_{1/2}$	A	13 815.2	—	—	—
$^4F_{9/2}$	A	21 002.5	20 993.5	20 999	21 026
	B	21 077.9	21 065.1	21 070	—
	C	21 103.4	21 088.9	21 093	21 097
	D	21 271.6	21 283	21 288	—
	E	21 278.4	21 299.8	21 304	21 249
$^4I_{15/2}$	A	22 051.0	22 066.1	22 070	22 104
	B	22 094.9	22 091.6	22 099	22 123
	C	22 096.7	22 097	22 153	22 153
	D	22 221.0	22 200	22 188	22 232
	E	22 275.7	22 287	22 202	22 321
	F	22 328.3	22 330	22 291	22 391
	G	22 386.8	22 353.8	22 333	—
	H	22 420.5	—	22 361	—

[a] Present work.
[b] From [6].
[c] From [7].

a few measurements by using polarized light. An example is supplied by figure 2, which compares, in the region of the $^6H_{15/2} \rightarrow ^6 H_{11/2}$ transition, the 9 K spectrum measured with unpolarized light to those measured with light polarized along two orthogonal directions. Many strong lines for the light electric field orthogonal to the z axis either weaken or vanish for the field parallel to it. The inset shows that the peak at $\sim$6046.9 cm^{-1} is broad in the unpolarized spectrum, but splits into two lines at 6046.73 and 6047.96 cm^{-1}, if the measurements are performed with light polarized along the z and y axis, respectively. The two lines (E1 and F1, see below) are due to transitions from the lowest sublevel of the ground $^6H_{15/2}$ manifold to two different sublevels of the excited $^6H_{11/2}$ manifold. Thus the polarized spectra were exploited as an additional tool for the correct line assignment in regions where the unpolarized spectra were rather complex.

The experimental line positions, measured at 9 K, are collected in table 1 and compared to those given in [6] and [7]. For most of the lines the positions listed in table 1 are the same for the two Dy concentrations investigated and for different crystal cuts, see figure 3. The lines are labelled Xi, where $i = 1, 2, 3, \ldots, 8$ indicates the sublevel of the ground manifold from which the absorption transition starts and $X = A, B, C, \ldots$ is related to the final sublevel in a given excited manifold. The positions of the ground state sublevels, reported in table 1, were derived by analysing the transitions starting from the thermally populated excited sublevels. For this purpose, the spectra were measured at different temperatures between 9 K and room temperature (by 20 K steps between 20 and 240 K). Figure 1 portrays, as an example, the $^6H_{15/2} \rightarrow ^6H_{13/2}$ transition for the 1% Dy:YAB. By increasing the temperature the amplitude of lines, attributed to transitions starting from the lowest sublevel of the ground $^6H_{15/2}$ manifold, showed a continuous decrease (X1 lines in figure 1); the same trend was observed for the areas subtended to the lines. In contrast, by increasing the temperature the areas under the lines,

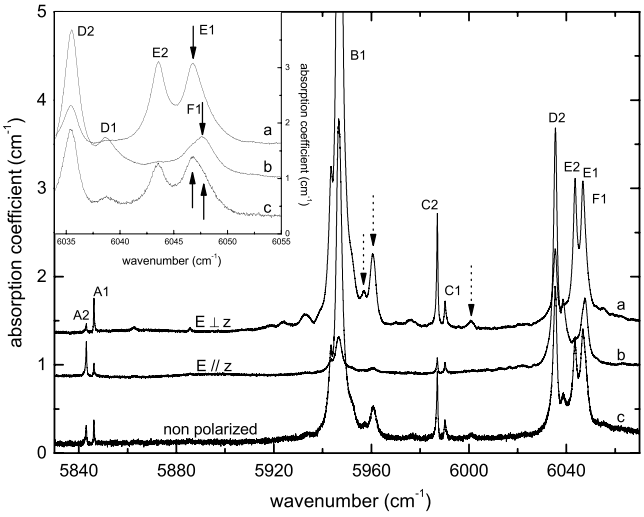

Figure 2. Absorption spectra of 1% Dy:YAB sample (x-cut) in the region of the $^6H_{15/2} \rightarrow {}^6H_{11/2}$ transition measured at 9 K with polarized and unpolarized light. Curves a and b, polarized spectra with the electric field E orthogonal and parallel to z axis crystallographic directions, respectively (resolution: 0.04 cm^{-1}). Curve c, unpolarized spectrum (resolution: 0.04 cm^{-1}). The inset shows a magnification in the 6034–6055 cm^{-1} range. The arrows indicate the E1 and F1 lines. The dotted arrows indicate some additional lines.

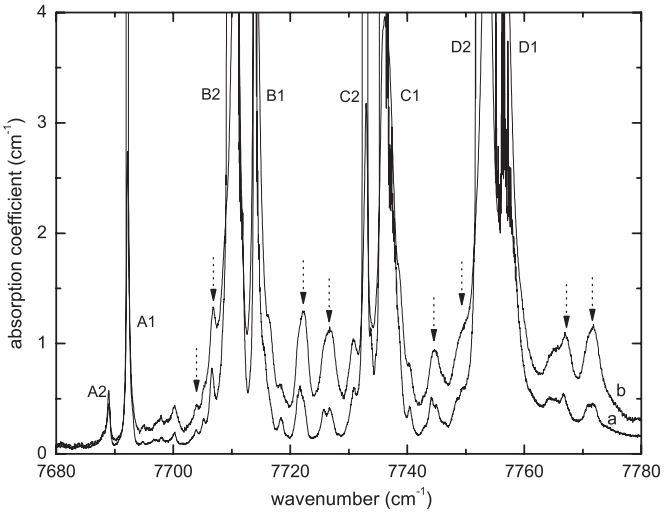

Figure 3. Absorption spectra of YAB samples doped with different Dy concentrations and crystal cuts measured at 9 K the region of the $^6H_{15/2} \rightarrow {}^6H_{9/2} + {}^6F_{11/2}$ transition (resolution: 0.04 cm^{-1}). Curve a, 4% Dy:YAB sample (z-cut); curve b, 1% Dy:YAB sample (x-cut). The dotted arrows indicate some additional lines.

attributed to transitions starting from the excited sublevels of the ground $^6H_{15/2}$ manifold, were characterized by an initial increase followed by a decrease (Xi lines, with $i = 2, 3$ in figure 1).

An interesting feature displayed by the 9 K spectra is represented by pairs of lines of comparable amplitude and separated only by ∼3.3 cm^{-1}. An example of them are the

3567.85–3570.98, 3576.66–3579.76 and 3595.02–3598.18 cm^{-1} pairs, respectively, shown in the 9 K curve in figure 1(a). By increasing the temperature from 9 to 20 K, within each pair the area under the low wavenumber line increases at the expense of the high wavenumber one. An example of such a behaviour is displayed in figure 1(a) by B2 and B1 lines at 3576.66 and 3579.76 cm^{-1}, respectively; compare curves a and b. This indicates that within each pair the former is related to a transition starting from the first excited sublevel of the ground manifold (X2 line), while the latter to a transition starting from the lowest sublevel (X1 line). Their small separation (3.3 ± 0.2 cm^{-1}, a value averaged over 26 pairs) justifies that the former line is rather strong at 9 K, being the first excited sublevel already populated. The splitting, in good agreement with the calculated one (see below and table 1), could be easily measured thank to the high resolution spectroscopy applied at low temperatures. In addition to the temperature dependence, the amplitude of the split components shows also a dependence on the light polarization direction, as already reported in [6], due to the YAB uniaxial crystal structure, compare, for example, in figure 2 the behaviour of the A1 and A2 lines (at 5846.18 and 5843.0 cm^{-1}, respectively).

At $T \geqslant 80$ K new lines were detected on the low wavenumber side of the X1 lines, being separated from them by $\sim$63 cm^{-1}: they are due to transitions starting from the second excited sublevel of the ground manifold (X3 lines), see as an example figure 1(b). The $\sim$63 cm^{-1} separation from the X1 lines (62.9 ± 1.9 cm^{-1}, a value averaged over 21 X1–X3 pairs) is in good agreement again with the calculated one (see below and table 1).

Some of the spectral lines are very narrow at 9 K: for example the half maximum at full width (HMFW) of the B1 line at 3579.76 cm^{-1} is 0.34 cm^{-1}; see figure 1. They broaden and shift by increasing the temperature, as shown in figure 1. The blue- or red-line shift of the line with temperature can be related to some lattice expansion, not necessarily isotropic, which changes the crystal field experienced by the rare-earth ions in a nontrivial way. The line sharpness at 9 K suggests that most of the Dy^{3+} ions are homogeneously incorporated in one specific site, i.e. the trigonal prismatic Y positions, without significant perturbation, at least for low Dy concentrations. A line broadening is indeed observed at 9 K, by increasing the Dy concentration from 1 to 4%: for example, the HMFW of the B1 line at 3579.76 cm^{-1} increases from 0.34 to 0.63 cm^{-1}. This means that the crystal field changes slightly if the separation between two Dy ions decreases by increasing the dopant concentration. A random distribution of Dy–Dy distances causes a line broadening. The concentration induced line broadening is in agreement with the observed excited lifetime shortening [6].

Furthermore, some weaker additional lines were detected, practically in all the spectral ranges where Dy^{3+} displays the above described main lines. Some examples of these are indicated by dotted arrows in figures 1–3. A tentative interpretation of their origin can be found by assuming that a minor part of the Dy^{3+} ions is located in sites where the lattice periodicity is altered. The crystal field around Dy^{3+} might be perturbed by the presence in the neighbourhood either of some unwanted impurity (examples are Mo, Cr, ... see above) or of other Dy ions. Location of Dy either at the interface between twinned regions or in areas affected by a possible local departure from stoichiometry (or by strains) might also induce an energy level scheme slightly different from that of Dy in unperturbed sites. Notwithstanding the fact that the 4f electrons are efficiently screened from the surroundings, the related crystal field transition energies can be finely tuned, for example by the presence of other rare earths, as already reported in the case of Er-doped BaY_2F_8 [20].

The energy levels of Dy^{3+} in YAB, determined by means of high resolution spectroscopy, were fitted with the theoretical procedure described in the previous section. The starting values of the free-ion and crystal-field parameters were those resulting from a previous investigation of the same material [7]. As regards the free-ion Hamiltonian, only the Coulombic parameters

Table 2. Free-ion and crystal-field parameters for Dy^{3+} and Er^{3+} in YAB. The values reported in square brackets were kept fixed during the fitting procedure.

Parameter	Value Dy (cm^{-1})	Value Er (cm^{-1})
E_{av}	56 035	35 574
F^2	91 025	96 329
F^4	63 864	68 001
F^6	49 462	53 342
ζ	1904.7	2369.6
α	[18]	[17.8]
β	[−633]	[−582]
γ	[1790]	[1800]
T^2	[329]	[400]
T^3	[36]	[43]
T^4	[127]	[73]
T^6	[−314]	[−271]
T^7	[404]	[308]
T^8	[315]	[299]
M^0	[3.39]	[3.86]
M^2	[1.90]	[1.93]
M^4	[1.05]	[1.29]
P^2	[719]	[594]
P^4	[359.5]	[297]
P^6	[71.9]	[59.4]
B_2^0	505	530
B_4^0	−1495	−1297
B_4^3	−814	−632
B_6^0	283	214
B_6^3	−75	−97
B_6^6	−244	−175

and the spin–orbit coupling were varied freely during the fitting procedure in order to avoid over-parametrization, due to the fact that all the fitted levels for this ion essentially belong to three terms only (^{6}H, ^{6}F and ^{4}I). The calculated energy levels are listed in table 1 together with the experimental ones; the fitting quality is very good and even significantly improved with respect to [7], as witnessed by its lower RMS deviation ($\sigma \approx 9$ cm^{-1}). This confirms that high resolution spectra can be important in assessing the crystal-field parameters. The sign and order of magnitude of the obtained theoretical parameters do not differ from [7], but the values of the crystal-field parameters (in particular B_2^0, which is about 30% larger than the previous value) have been significantly corrected (table 2).

Interestingly, the presence of a pseudo-quartet ground state (the two lowest energy levels being two weakly separated Kramers doublets), which was suggested in a previous work [7] but could not be confirmed or disproved directly due to the resolution limits of the spectrometers used, was experimentally detected in the high resolution spectra. The measured value of the gap (3.3 ± 0.2 cm^{-1}) is consistent with the calculated one.

Following the results of the present calculations, we attempted to classify the energy states in the range 7600–9400 cm^{-1} (where the ^{6}H and ^{6}F terms are overlapping) according to the major component of their wavefunctions; however, in almost all cases the overlap gives rise to heavily mixed ^{6}H + ^{6}F states, making the separation of the two terms impossible.

Table 3. Comparison between the theoretical (present work) and experimental values of Er^{3+} energy levels (cm^{-1}) in YAB crystals for different $^{2S+1}L_J$ manifolds. The experimental values are taken from [8–10], as indicated.

$^{2S+1}L_J$	Level	Theoretical	Exp.	Reference	$^{2S+1}L_J$	Level	Theoretical	Exp.	Reference
$^4I_{15/2}$	1	−10	0	[8–10]	$^2H_{11/2}$	A	19 150	19 119	[9]
	2	33	47			B	19 152	19 127	
	3	95	109			C	19 186	19 164	
	4	125	128			D	19 224	19 227	
	5	162	157			E	19 249	19 256	
	6	269	244			F	19 261	19 272	
	7	288	287		$^4F_{7/2}$	A	20 477	20 478	
	8	293	316			B	20 505	20 506	
$^4I_{13/2}$	A	6539	6527	[8]		C	20 580	20 595	
	B	6573	6561			D	20 604	20 614	
	C	6624	6611		$^4F_{5/2}$	A	22 158	22 165	
	D	6640	6639			B	22 177	22 187	
	E	6729	6724			C	22 220	22 244	
	F	6742	6735		$^4F_{3/2}$	A	22 509	22 517	
	G	6749	6740			B	22 577	22 586	
$^4I_{11/2}$	A	10 204	10 210		$^2H_{9/2}$	A	24 533	24 568	[10]
	B	10 228	10 230			B	24 559	24 591	
	C	10 263	10 264			C	24 615	24 636	
	D	10 303	10 300			D	24 637	24 657	
	E	10 313	10 311			E	24 679	24 765	
	F	10 320	10 349		$^4G_{11/2}$	A	26 319	26 298	
$^4I_{9/2}$	A	12 411	12 428	[9]		B	26 336	26 313	
	B	12 428	12 460			C	26 392	26 373	
	C	12 508	12 498			D	26 484	26 485	
	D	12 529	12 547			E	26 514	26 508	
	E	12 581	12 578			F	26 530	26 543	
$^4F_{9/2}$	A	15 223	15 206		$^4G_{9/2}$	A	27 375	27 377	
	B	15 305	15 291			B	27 396	27 400	
	C	15 358	15 349			C	27 410	27 418	
	D	15 384	15 368			D	27 434	27 455	
	E	15 394	15 395			E	27 454	27 501	
$^4S_{3/2}$	A	18 367	18 367						
	B	18 416	18 418						

Table 1 shows that the energy levels, as obtained from the present experiments, are in better agreement with the theoretical calculations than those of [6] and [7]. We attribute this progress to the high resolution spectra and to their detailed polarization and temperature dependence analysis.

3.2. YAB:Er

The same theoretical method was applied to obtain the free-ion and crystal-field parameters of YAB:Er^{3+}, by using previously published high resolution experimental data in the IR and visible range [8, 9] as the basis for the fitting procedure. A good fitting ($\sigma \approx 13$ cm^{-1}) is obtained and the calculated energy levels are compared to the experimental ones in table 3. The resulting crystal-field parameters (table 2) are quite close to those obtained for YAB:Dy^{3+}, as expected for different rare-earth ions substituting Y in the same host crystal [21]. The slight

difference in the fourth- and sixth-order parameters (roughly 20% smaller for erbium) can be attributed to the different radial extension of the $4f^9$ and $4f^{11}$ wavefunctions [22]. Again, while the sign and order of magnitude of the present crystal-field parameters do not differ much from those obtained by analysing standard-resolution data [11], quantitative differences between the high-order parameters can be noticed, and the present set is in better agreement with the one obtained independently for Dy in the same host. The present parameters were also used to predict the position of the energy levels up to 27 500 cm^{-1}, which were then compared to those arising from a previous standard-resolution investigation [10]; once again a satisfactory agreement between theory and experiment is found.

4. Conclusions

High resolution absorption spectra of Dy-doped YAB were monitored. The resulting energy levels were fitted by a theoretical crystal-field model, which was also applied to fit previously published high resolution data for YAB:Er. A good agreement between theory and experiment was obtained in both cases. Very similar crystal-field parameters B_k^q were found for Dy and Er, as expected when dealing with different rare earth ions embedded in the same host, notwithstanding the fact that fitting procedures were carried on independently. This is a strong argument in favour of the reliability of the present analysis, together with the fact that the calculated levels outside the high resolution energy limit (not included in the fitting procedure) reasonably agree with the results of standard-resolution experiments for Er. To summarize, the exploited D_3 Hamiltonian correctly describes the experimental data; this is an indirect confirmation that most of the trivalent rare-earth ions enter YAB by substituting Y in its trigonal prismatic site. In particular, the new spectra collected for YAB:Dy samples made it possible to improve the theoretical analysis, solving some discrepancies in the previously published line positions and attributions. Moreover, a direct experimental confirmation of the quasi-quartet ground state suggested in [7] could be given thanks to the high resolution, with a measured gap between the two lowest Stark doublets of $\sim$3.3 cm^{-1}, which is also consistent with the present crystal-field model.

Acknowledgments

The present work has been supported by a CNR-HAS joint project, a Hungarian–Italian intergovernmental R&T project, the Hungarian Research Fund OTKA T-46481 and the Italian MIUR. The authors want to thank Mr Carlo Mora (IMEM-CNR–Parma) for technical help and Dr Lorenzo Venturi for some measurements.

References

[1] Filimonov A A, Leonyuk N I, Meissner L B, Timchenko T I and Rez I S 1974 *Krist. Tech.* **9** 63
[2] Cavalli E, Speghini A, Bettinelli M, Ramirez M O, Romero J J, Bausa L E and Garcia Sole J 2003 *J. Lumin.* **102/103** 216
[3] Földvári I, Beregi E, Baraldi A, Capelletti R, Ryba-Romanowski W, Dominiak-Dzik G, Munoz A and Sosa R 2003 *J. Lumin.* **102/103** 395
[4] Chinn S R and Hong H Y-P 1975 *Opt. Commun.* **15** 345
[5] Lu B, Wang J, Pan H, Jiang M, Liu E and Hou X 1989 *J. Appl. Phys.* **66** 6052
[6] Dominiak-Dzik G, Solarz P, Ryba-Romanowski W, Beregi E and Kovács L 2003 *J. Alloys Compounds* **359** 51
[7] Cavalli E, Bovero E, Magnani N, Ramirez M O, Speghini A and Bettinelli M 2003 *J. Phys.: Condens. Matter* **15** 1047
[8] Földvári I, Beregi E, Capelletti R, Baraldi A, Munoz A and Sosa R 2003 *Radiat. Eff. Defects Solids* **158** 285

[9] Földvári I, Beregi E, Capelletti R and Baraldi A 2005 *Phys. Status Solidi* c **2** 260
[10] Földvári I, Beregi E, Munoz A, Sosa R and Horváth V 2002 *Opt. Mater.* **19** 241
[11] Dammak M 2005 *J. Alloys Compounds* **393** 51
[12] Beregi E, Hartmann E, Malicskó L and Madarász J 1999 *Cryst. Res. Technol.* **34** 641
[13] Bencs L, Horváth V, Varga I, Beregi E and Kántor T 2004 *Spectrochim. Acta* B **59** 1851
[14] Wang G, Gallagher H G, Han T P J and Henderson B 1996 *J. Cryst. Growth* **163** 272
[15] Dominiak-Dzik G, Ryba-Romanowski W, Grinberg M, Beregi E and Kovács L 2002 *J. Phys.: Condens. Matter* **14** 5229
[16] Péter Á, Polgár K and Beregi E 2000 *J. Cryst. Growth* **209** 102
[17] Carnall W T, Goodman G L, Rajnak K and Rana R S 1989 *J. Chem. Phys.* **90** 3443
[18] Crosswhite H M and Crosswhite H 1984 *J. Opt. Soc. Am.* B **1** 246
[19] Wybourne B G 1965 *Spectroscopic Properties of Rare Earths* (New York: Interscience)
[20] Baraldi A, Capelletti R, Mazzera M, Ponzoni A, Amoretti G, Magnani N, Toncelli A and Tonelli M 2005 *Phys. Rev.* B **72** 075132
[21] Newman D J and Ng B 2000 *Crystal Field Handbook* (Cambridge: Cambridge University Press)
[22] Freeman A J and Desclaux J P 1979 *J. Magn. Magn. Mater.* **12** 11